Optimal Doping Control of Magnetic Semiconductors via Subsurfactant Epitaxy

Changgan Zeng,[1] Zhenyu Zhang,[2,1] Klaus van Benthem,[2] Matthew F. Chisholm,[2] and Hanno H. Weitering[1,2]

[1]*Department of Physics and Astronomy, The University of Tennessee, Knoxville, Tennessee 37996, USA*

[2]*Materials Sciences and Technology Division, Oak Ridge National Laboratory, Oak Ridge, Tennessee 37831, USA*

(Received 18 January 2007; revised manuscript received 4 December 2007; published 12 February 2008)

''Subsurfactant epitaxy'' is established as a conceptually new approach for introducing manganese as a magnetic dopant into germanium. A kinetic pathway is devised in which the subsurface interstitial sites on Ge(100) are first selectively populated with Mn, while lateral diffusion and clustering on or underneath the surface are effectively suppressed. Subsequent Ge deposition as a capping layer produces a novel surfactantlike phenomenon as the interstitial Mn atoms float towards newly defined subsurface sites at the growth front. Furthermore, the Mn atoms that failed to float upwards are uniformly distributed within the Ge capping layer. The resulting doping levels of order 0.25 at. % would normally be considered too low for ferromagnetic ordering, but the Curie temperature exceeds room temperature by a comfortable margin. Subsurfactant epitaxy thus enables superior dopant control in magnetic semiconductors.

DOI: 10.1103/PhysRevLett.100.066101 PACS numbers: 68.55.Ln, 75.70.−i

Dilute magnetic semiconductors (DMS) have attracted tremendous interest both experimentally [1,2] and theoretically [3,4] due to their vast potential for advancing spin-based electronics or ''spintronics'' [5]. Their magnetic properties can be controlled by intentional introduction of magnetic impurities. For practical purposes, ferromagnetism above room temperature would be highly desirable, but research efforts aimed at reaching this goal typically invoked the use of excessive impurity concentrations of at least a few percent. Such high doping levels are detrimental to the structural homogeneity [6–8] and carrier mobility of most semiconductors, while clustering of impurities limits the experimentally achievable ferromagnetic ordering temperature T_C [9].

In this Letter, we report the discovery of ''subsurfactant epitaxy'' as a conceptually new approach for introducing Mn into Ge to achieve a Si-compatable DMS with high magnetic ordering temperatures. A kinetic pathway is devised in which the subsurface interstitial sites on Ge(100) are first populated with Mn, while lateral diffusion and clustering on or underneath the surface are effectively suppressed. When the Mn-decorated Ge surface is covered by subsequent Ge deposition, most of the interstitial Mn atoms float towards newly defined subsurface sites at the growth front. The small fractions of Mn atoms that failed to float upwards are uniformly distributed within the Ge epilayer. The resulting films have Mn doping levels of order 0.25 at. %, but the observed $T_C > 400$ K exceeds room temperature by a comfortable margin.

The key toward this superior doping control is rooted in two conceptually related developments in nonequilibrium growth. The first is the well-known surfactant action in heteroepitaxy, referring to the intriguing phenomenon that a low dose of a third element C serving as a surface active agent (the surfactant) on the substrate B can drastically improve layer-by-layer growth of element A [10]. Despite many research efforts since the initial discovery, surfactant epitaxy still has limited technological appeal, primarily because the amounts of surfactant atoms unavoidably trapped inside the films are too high to be tolerable for most electronic applications [11]. This apparent drawback in surfactant epitaxy nonetheless inspires us to explore the feasibility of introducing magnetic dopants into semiconductors within the spirit of surfactant action and trapping. The second development is the recent theoretical prediction of ''subsurfactant'' action of Mn on Ge(100), referring to the strong preference of predeposited Mn atoms to occupy subsurface interstitial sites located between the two topmost Ge layers, and their predicted ability to float towards newly defined subsurface sites upon deposition of additional Ge epilayers [12]. The natural question then is ''Can a desirable amount of Mn be trapped inside the Ge epilayer during subsurfactant action, much like the unintentional trapping in surfactant epitaxy, so as to produce better quality DMS?'' A confirming answer is provided below, along with evidence for surprisingly strong ferromagnetism.

Samples were prepared in ultrahigh vacuum. Ge(100) substrates were cleaned *in situ* by cycles of sputtering and annealing. A thin Ge buffer layer was grown at 400 °C so as to produce a high quality substrate with a well-ordered (2×1) surface reconstruction. Mn and Ge were deposited from thermal effusion sources and the deposition rates were calibrated with scanning tunneling microscopy (STM) and *ex situ* Rutherford backscattering spectrometry (RBS). For *ex situ* investigations, samples were capped with an amorphous Ge layer deposited at 170 K.

Subsurfactant growth involves two steps. Step 1 entails deposition of a submonolayer amount of Mn onto the clean Ge(100)2×1 buffer layer at ~150 K. At this temperature, a majority of Mn atoms occupy subsurface interstitial sites, as predicted recently [12] and experimentally confirmed here. This is illustrated in Fig. 1(a), which shows the STM image after deposition of 0.05 ML Mn on a flat buffer layer

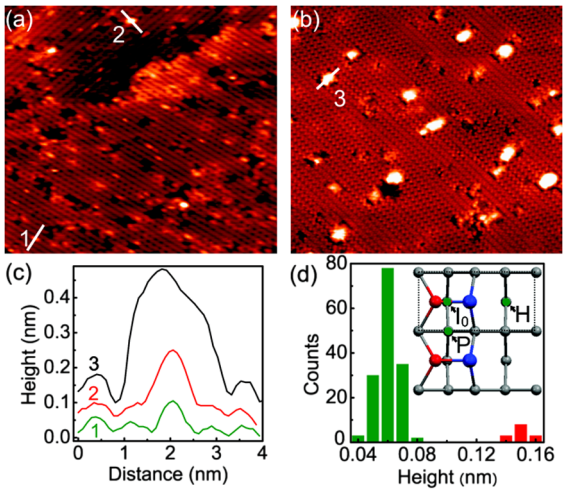

FIG. 1 (color online). (a) and (b) are STM images of 0.05 ML Mn on Ge(100) deposited at ~150 K and RT, respectively. For both figures, the image size is 35 nm × 32 nm, and the sample bias is −1.2 V.(c) Profiles along the topographic lines of the Mn-induced bright features shown in (a) and (b). (d) Statistical height distribution of the Mn-induced features from STM images on the LT sample. The inset is a top view of the Ge(100) − (2 × 1) surface. The blue or gray (red or dark gray) circles represent the up (down) atoms of Ge-Ge dimers on the surface.

at 150 K. The image is dominated by Mn-induced bright features, which are absent on the clean Ge(100) surface. Their line scans ["1" and "2" in Fig. 1(a)] are compared in Fig. 1(c). These feature sizes exhibit a bimodal distribution centered at 0.6 and 1.5 Å [Fig. 1(d)]. The 0.6 Å features are in lateral registry with the dimer rows of the 2 × 1 surface reconstruction and account for ~90% of the adsorption-induced features. Their vertical protrusions are too low for atop adatoms and must be attributed to Mn atoms occupying the preferred interstitial sites I_0, located underneath the Ge surface dimers as indicated in the inset of Fig. 1(d) [12]. The image is consistent with theoretical STM simulations for Mn at the I_0 sites on Si(100) [13]. The 1.5 Å minority features are consistent with the apparent height of isolated adatoms, and are located either on top or between the dimer rows; these features can be attributed to Mn adatoms occupying the pedestal (P) or hollow sites (H) of the 2 × 1 surface reconstruction as illustrated in Fig. 1(d). Deposition of 0.5 ML Mn at LT (low temperature) results in a $c(4 \times 2)$ reconstruction, consistent with the fact that the areal density of Ge dimers on the clean Ge(100)-$c(4 \times 2)$ reconstruction is also 0.5 ML.

Low temperature predeposition is essential for trapping Mn at the subsurface interstitial sites, which in turn prevents Mn clustering. Based on first-principles calculations [12], Mn adatoms occupying the metastable H or P sites can easily dive into the I_0 sites but the reverse process requires overcoming an energy barrier of over 1 eV. Therefore, once a Mn adatom dives into an I_0 site, it is unlikely to hop back to atop sites at the low deposition temperature. Such efficient trapping of Mn dopants at the subsurface sites reduces the monomer density on the surface, thereby suppressing the lateral diffusion and formation of Mn clusters. On the other hand, room temperature deposition reduces the trapping efficiency and facilitates cluster formation, as illustrated by the larger and brighter features in Fig. 1(b). The vertical height of those features is about 3 Å, as indicated by line scan "3" in Figs. 1(b) and 1(c). Such contrasting behavior is observed even for a Mn deposit up to 0.5 ML coverage (not shown), i.e., Mn atoms are uniformly distributed with LT deposition, while they form clusters in the case of RT (room temperature) deposition.

The second step of subsurfactant epitaxy involves subsequent deposition of pure Ge epilayers on the Mn-dosed Ge substrates. We performed experiments with Mn predeposited at room temperature and at 150 K. The substrate is warmed to 85 °C, high enough to allow epigrowth but still low enough to avoid formation of intermetallic precipitates [9]. The inset of Fig. 2(a) shows the corresponding reflection high energy electron diffraction pattern of a LT sample with an initial Mn deposit of 0.5 ML and a 20-nm-thick Ge layer. The pattern indicates that the Ge layer is crystalline and that the (2 × 1) surface reconstruction is preserved.

To monitor the upward floating capability of individual Mn atoms, we interrupted the Ge growth repeatedly to measure the Mn 2p core level intensity with x-ray photoelectron spectroscopy [XPS; Fig. 2(a)]. The Mn intensity of the 0.5 ML RT sample decreases sharply within the first 4 nm of Ge deposition. Because XPS is surface sensitive, it indicates that the Mn clusters initially formed at the inter-

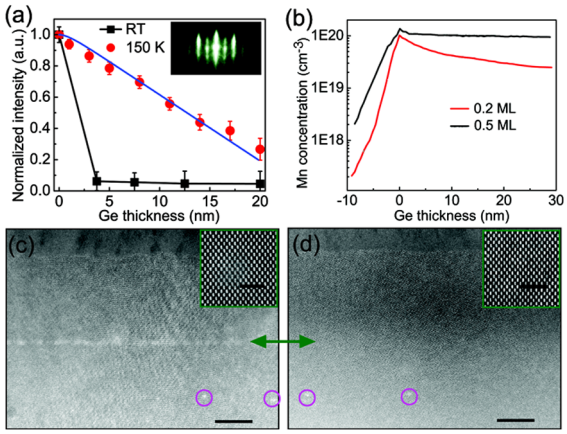

FIG. 2 (color online). (a) Integrated Mn 2p core level intensity as a function of Ge epilayer thickness for the 0.5 ML RT and LT samples. (b) SIMS results for the LT samples with initial deposits of 0.2 and 0.5 ML. The vertical line at 0 nm indicates the location of the interface between the Ge buffer layer and Ge epilayer. (c) and (d) are cross-sectional STEM images of RT and LT samples with 0.5 ML of Mn, respectively. The interface between the Ge buffer layer and epilayer is indicated by the double pointed arrow. Scale bars in both images correspond to 20 nm. The insets of (c) and (d) are higher magnification images. All four images were acquired under the same resolution conditions. The scale bars in both insets correspond to 2 nm.

face are immobilized deep inside the Ge epilayer. In contrast, the Mn $2p$ intensity of the 0.5 ML LT samples decays much more slowly with increasing epilayer thickness. XPS thus confirms the upward floating of the Mn atoms during Ge growth; the slow decay also provides direct evidence for dopant trapping inside the film. The blue (or gray) line in Fig. 2(a) is a fit using a simple layer-by-layer attenuation scheme for the Mn XPS intensity, assuming that a small but *constant amount* of Mn is trapped inside each Ge layer as the growth front advances (fitting with a *constant fraction* of trapping from layer to layer yielded poorer agreement). The inelastic mean free path of the photoelectrons used is 1 nm [14]. This fitting produces a Mn concentration of 0.25%, a finding that is independently confirmed by secondary ion mass spectrometry (SIMS) of the 0.5 ML sample as shown in Fig. 2(b), where the doping level decays only slightly (from 1.09×1020 Mn atoms per cm^3 at the buffer-layer interface to 0.95×10^{20} cm^{-3} at 35 nm above the interface). The average doping concentration is 1.02×10^{20} Mn atoms per cm^3, or 0.23%, in excellent agreement with the XPS result. The constant Mn profile may be due to a nearly constant kinetic solubility established at the given growth conditions [15]. The doping profile of the 0.2 ML LT sample also reveals the upward floating phenomenon, resulting in an overall lower but less constant doping level [Fig. 2(b)].

Scanning transmission electron microscopy (STEM) investigation provides the final cross check of the spatial distribution of the Mn dopants. We examined cross sections of the RT and LT samples, prepared by mechanical polishing and followed by 0.5–2.0 kV argon milling. The images were recorded using an aberration-corrected VG HB603 U STEM operated at 300 kV. Low-angle (35 mrad) annular dark field images of the RT and LT samples are shown in Figs. 2(c) and 2(d), respectively. The initial Mn deposit is 0.5 ML in both cases. We can precisely locate the interface between the Ge substrate and the buffer layer by tracking a line of defects at this interface with STEM as indicated by the circles in Figs. 2(c) and 2(d). Therefore we can be confident that the RT and LT samples have identical Ge buffer and epilayer structures. Figure 2(c) reveals bright clusters at the buffer-layer–epilayer interface of the RT sample. The contrast disappears when the inner annular dark field detector angle is increased to 50 mrad, indicating that the contrast is due to strain at the cluster/matrix interface [16]. No Mn-Ge clusters have been observed inside the epilayer of either material (RT and LT) over extended distances along the epilayer–buffer-layer interface.

Electron energy loss spectroscopy (EELS) was performed using an aberration-corrected VG HB501 UX STEM operated at 100 keV, equipped with a Gatan Enfina parallel EELS system. EELS spectra (not included) show that the clusters at the buffer-layer–epilayer interface of the RT sample contain trapped Mn. No such clusters have been detected at the similar interface of the LT sample [Fig. 2(d)], indicating that the Mn atoms have been incorporated into the epilayer. Because of the small concentration of Mn atoms in the epilayer (approximately 0.25%), i.e., below the detection limit for STEM-EELS in the used alignment, the Mn signal recorded from the epilayer remained below the noise level in recorded EELS data.

To summarize the growth part, STM, XPS, SIMS, and STEM are consistent and collectively depict the novel mode of "subsurfactant epitaxy": predeposited Mn atoms occupy the subsurface interstitial I_0 sites at LT. Subsequently, these Mn dopants float towards the newly defined subsurface sites at the growth front upon deposition of new Ge epilayers. A small fraction of the upward diffusing Mn atoms is unavoidably trapped inside the Ge matrix, similar to the case of surfactant epitaxy [11], resulting in a homogeneous Mn-doped Ge thin film. The trapped Mn atoms are most likely located in substitutional lattice sites, which are ultimately the most favorable sites [12].

Next, we focus on the magnetic properties measured with SQUID magnetometry. Figure 3(a) shows the remanent magnetization as a function of temperature for the LT samples with different initial Mn coverages. It indicates that for LT samples, the ferromagnetic ordering temperature T_C scales with the initial Mn coverage. For the 0.1 and 0.2 ML samples, T_C is 150 and 330 K, respectively. For the 0.5 ML sample, T_C exceeds the temperature capability of the cryostat, i.e., $T_C > 400$ K. We recall that the doping concentration of the 0.5 ML sample is only 0.23%. Considering these low doping concentrations, the magnetic ordering temperatures represent an unexpectedly large improvement over those of Mn_xGe_{1-x} films grown by MBE codeposition [6,7,9]. Magnetization loops of the 0.5 ML sample are shown in Fig. 3(b). The saturation magnetization at 2 K is about $2.8\mu_B$ per Mn, close to the theoretical value of $3\mu_B$ for substitutional Mn [2,17]. The coercivity is very small, about 80 Oe. Dopant clustering has an adverse effect on the magnetic properties: the remanent magnetization of the 0.5 ML RT sample disappears at 50 K [Fig. 3(a)], while the net magnetic moment is also reduced.

One most crucial issue in DMS research is whether the observed magnetism is intrinsic, induced by substitutional Mn, or extrinsic, caused by unintentional contamination or clustering of dopants. STEM did not produce evidence for clustering in LT samples since no strain contrast was

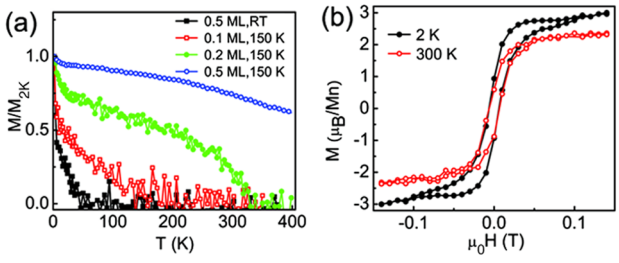

FIG. 3 (color online). (a) Temperature dependence of the normalized remanent magnetization for different deposition temperatures and different Mn coverages. (b) Magnetic hysteresis loops of a LT sample with 0.5 ML of Mn. The Ge epilayer thickness for all samples is 35 nm.

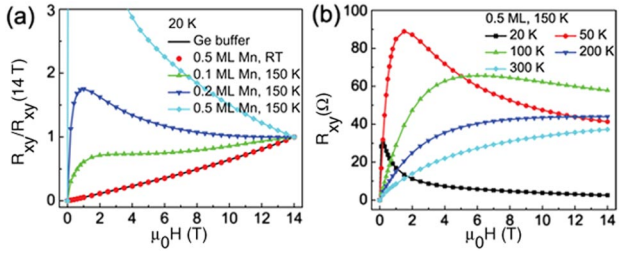

FIG. 4 (color online). (a) Hall effect measured at 20 K for different initial Mn coverages and different growth temperatures. The Ge epilayer thickness is 35 nm. The Hall effect of the Ge buffer layer is also shown for reference. (b) Hall effect of the LT sample with 0.5 ML initial coverage, measured at various temperatures.

observed. We performed SIMS analysis on several samples to check for the presence of spurious magnetic elements such as Fe, Co, and Ni. Fe is the main metal contaminant. However, the Fe content is at least 3 orders of magnitude lower than that of Mn, far too low to account for the measured magnetic moment. We also found traces of the usual *C*, *N*, and *O* contaminants; none of these could significantly affect the magnetic properties. Instead, we attribute the contrasting magnetism of the RT and LT samples to their different Mn profiles.

To further explore the ferromagnetic nature of the LT sample, we measured the anomalous Hall effect (AHE), using a Hall bar and averaging the Hall voltages for positive and negative magnetic fields. To minimize parallel conduction through the bulk substrate, we grew the Ge buffer layer on GaAs. The LT samples exhibit a strong AHE that increases with Mn content [Fig. 4(a)]. It can be observed up to at least 300 K for the LT sample with 0.5 ML initial Mn coverage [Fig. 4(b)], consistent with the SQUID measurements in Fig. 3. In contrast, the RT samples do not exhibit an AHE.

The AHE of the LT sample is consistent with that of a ferromagnetic DMS. Its scaling with Mn content, along with the negligible amounts of spurious impurities in SIMS seems to rule out bulk- or edge contaminants as the source of the SQUID and AHE signals. Finally, it is noted that the high-field slopes in the Hall effect changes with temperature, a commonly observed phenomenon in DMS, which precludes reliable determination of the carrier density [9,18].

How can such a diluted system exhibit high T_C? Extensive cross checks for spurious phenomena turned out negative, and thus the coupling mechanism is possibly intrinsic. It certainly differs from the itinerant exchange in III-V DMS, which requires metallic doping levels. Our findings are more in line with reports on high-T_C ferromagnetism in insulating DMS, including dilute oxide and nitride systems [19–21]. This suggests an interesting commonality between these seemingly different DMS systems.

In summary, we established ''subsurfactant epitaxy'' as a conceptually new kinetic pathway for incorporating Mn dopants in Ge. The resulting doping levels of order 0.25% are normally considered too low for establishing ferromagnetism, but T_C exceeds 400 K. This magnetism is possibly intrinsic in nature, though the origin of the ferromagnetic coupling remains to be determined. Subsurfactant epitaxy may also be useful for other semiconductor applications that require doping levels above the thermodynamic solubility limit.

We thank L. C. Feldman for the RBS measurements. This work was supported in part by NSF under Contract No. DMR-0606485, the U.S. Department of Energy (Grant No. DE-FG02-05ER46209), and the Division of Materials Sciences and Engineering, Office of Basic Energy Sciences, DOE, under Contract No. DE-AC05-00OR22725 with Oak Ridge National Laboratory, managed by UT-Battelle, LLC. K. v. B. acknowledges financial support from the Alexander von Humboldt Foundation.

[1] H. Ohno, Science **281**, 951 (1998).
[2] Y. D. Park *et al.*, Science **295**, 651 (2002).
[3] T. Dietl *et al.*, Science **287**, 1019 (2000).
[4] A. H. MacDonald, P. Schiffer, and N. Samarth, Nat. Mater. **4**, 195 (2005).
[5] I. Žutić, J. Fabian, and S. Das Sarma, Rev. Mod. Phys. **76**, 323 (2004).
[6] M. Jamet *et al.*, Nat. Mater. **5**, 653 (2006).
[7] C. Jaeger *et al.*, Phys. Rev. B **74**, 045330 (2006).
[8] D. Bougeard *et al.*, Phys. Rev. Lett. **97**, 237202 (2006).
[9] A. P. Li, J. Shen, J. R. Thompson, and H. H. Weitering, Appl. Phys. Lett. **86**, 152507 (2005); A. P. Li *et al.*, Phys. Rev. B **72**, 195205 (2005).
[10] M. Copel, M. C. Reuter, E. Kaxiras, and R. M. Tromp, Phys. Rev. Lett. **63**, 632 (1989).
[11] D. Kandel and E. Kaxiras, in *Solid State Physics*, edited by H. Ehrenreich and F. Spaepen (Academic Press, San Diego, 2000), Vol. 54, p. 219; D. Reinking, M. Kammler, M. Horn-von Hoegen, and K. R. Hofmann, Appl. Phys. Lett. **71**, 924 (1997).
[12] W. Zhu *et al.*, Phys. Rev. Lett. **93**, 126102 (2004).
[13] G. M. Dalpian, A. J. R. da Silva, and A. Fazzio, Phys. Rev. B **68**, 113310 (2003).
[14] C. J. Powell and A. Jablonski, J. Phys. Chem. Ref. Data **28**, 19 (1999).
[15] S. B. Zhang and S.-H. Wei, Phys. Rev. Lett. **86**, 1789 (2001).
[16] D. D. Perovic, C. J. Rossow, and A. Howie, Ultramicroscopy **52**, 353 (1993).
[17] Y.-J. Zhao, T. Shishidou, and A. J. Freeman, Phys. Rev. Lett. **90**, 047204 (2003).
[18] F. Tsui *et al.*, Phys. Rev. Lett. **91**, 177203 (2003).
[19] Y. Matsumoto *et al.*, Science **291**, 854 (2001).
[20] K. A. Griffin *et al.*, Phys. Rev. Lett. **94**, 157204 (2005).
[21] J. M. D. Coey, M. Venkatesan, and C. B. Fitzgerald, Nat. Mater. **4**, 173 (2005).